Identification of the donor and acceptor states of the bond-centered hydrogen–carbon pair in Si and diluted SiGe alloys

R. Stübner,[1] Vl. Kolkovsky,[1] J. Weber,[1,a] (ID) N. V. Abrosimov,[2] C. M. Stanley,[3] (ID) D. J. Backlund,[4] and S. K. Estreicher[5] (ID)

AFFILIATIONS

[1] Technische Universität Dresden, 01062 Dresden, Germany
[2] Leibnitz-Insitute for Crystal Growth, 12489 Berlin, Germany
[3] RB Annis School of Engineering, University of Indianapolis, Indianapolis, Indiana 46227, USA
[4] Simulation IT, Texas Tech Health Sciences Center, Lubbock Texas 79430-8317, USA
[5] Physics Department, Texas Tech University, Lubbock Texas 79409-1051, USA

Note: This paper is part of the Special Topic on Defects in Semiconductors 2020.
[a] **Author to whom correspondence should be addressed:** joerg.weber@tu-dresden.de

ABSTRACT

The electrical and structural properties of two levels (E90 and H180) in diluted n- and p-type $Si_{1-x}Ge_x$ alloys ($0 \leq x \leq 0.070$) are investigated by high-resolution Laplace deep level transient spectroscopy measurements and first-principles calculations. By exploiting the presence of Ge atoms close to a substitutional C atom, we show that E90 and H180 belong to the same C–H pair (labeled CH_{1BC}) with H in a bond-centered configuration (C—H_{BC}—Si). The relative energies of the various configurations of the CH pair are calculated, and the complete vibrational spectra in the lowest-energy structures for each charge state are predicted.

I. INTRODUCTION

Carbon and oxygen are the main contaminants in high-purity electronic-grade Si used in semiconductor devices. The presence of carbon in Si originates mainly from the polycrystalline source material. In the present work, we are interested in isolated substitutional carbon (C_s). It is electrically inactive, but the short C—Si bond length generates strain which attracts interstitials such as H. Typical C_s concentrations are between 10^{15} and $10^{17}\,cm^{-3}$ for crucible-pulled (CZ) and float-zone (FZ) Si, respectively. Isolated O is mostly the electrically inactive interstitial O_i.[1]

Hydrogen is commonly used for passivating interface states between silicon and gate oxides. It also forms electrically-active complexes with C_s. The properties of several CH pairs in Si have been studied extensively using Fourier-transform infrared absorption (FTIR) spectroscopy and deep level transient spectroscopy (DLTS).[2–7] Five *a priori* possible configurations of CH predicted by theory[6,8–10] are schematically shown in Fig. 1: CH_{1BC} with H near a bond-centered site between C_s and a neighboring Si atom; CH_{2BC}

with H at a bond-center site between two Si atoms neighboring C_s; CH_{1AB} with H anti-bonding to C_s; CH_{2AB} with H anti-bonding to a Si nearest-neighbor (NN) to C_s; and CH_T with H near the tetrahedral interstitial (T) site.

Experimental evidence exists for some of these configurations. After wet-chemical etching, a prominent DLTS peak E90 with a level position at EC−0.16 eV was observed in n-type FZ Si (E_c is the conduction band edge).[2,7,11] This level agrees with the calculated position of the single-acceptor state of CH_{1BC}. The nature of this defect was confirmed by combining Laplace DLTS (LDLTS) with uniaxial stress measurements.[6] The CH_{2BC} configuration has a level at EC−0.22 eV. It was observed only after low temperature hydrogen implantation.[6] CH_{2BC} is thermally unstable and anneals out at 225 K. Two more DLTS peaks E42 and E262 with level positions at EC−0.06 eV (E42) and EC−0.51 eV (E262) appear in hydrogenated n-type CZ- and FZ-Si samples.[12] Evidence was presented that these levels belong to the double-acceptor (E42) and single-acceptor states (E262) of CH_{1AB}. In hydrogenated p-type Si,
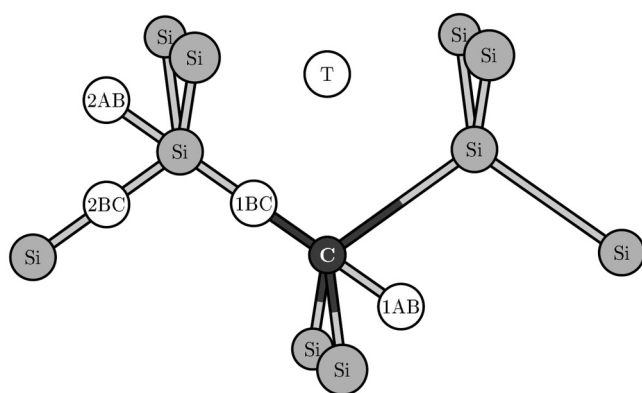
FIG. 1. *A priori* possible sites for H near C_s in Si.[6] BC means (near) bond-centered, AB anti-bonding, and T is the tetrahedral interstitial site.

the DLTS peak H180 with a level position at $E_V + 0.33$ eV was reported.[4] The independence of the level position on an applied electrical field associates this level to a donor state of a CH complex. However, the identification of this level with a specific configuration of the CH pair is controversial. From the annealing properties of E90 and H180, Kamiura *et al.* suggested that H180 could not be assigned to the donor state of CH_{1BC} but should be attributed to CH_{1AB}.[4] The same authors also speculated that H180 could be a CH pair that involves more than one H atom. In contrast, the calculations of Andersen *et al.*[6] show that CH_{1AB} has no donor level in the bandgap and that H180 should be attributed to the donor state of CH_{1BC}.

Structural information about these defects can be extracted in $Si_{1-x}Ge_x$ alloys. Indeed, alloying affects the defects in several ways. The reduction of the bandgap with increasing Ge content shifts the electronic levels. More importantly, the presence of different numbers of Ge atoms in the 1st and 2nd Si nearest-neighbor (NN) shells around C_s leads to the appearance of additional levels (alloy splitting) with slightly different electrical properties and thermal stabilities. Alloy splitting is only detectable by the high-resolution LDLTS technique.[13,14]

In this paper, we focus on the properties of the CH_{1BC} pair in *n*- and *p*-type Si and $Si_{1-x}Ge_x$ alloys with $0 \leq x \leq 0.070$ (preliminary experimental results have been published previously).[15,16] We give experimental support for the stability of the CH_{1BC} configuration. We also present the results of new calculations of the relative stability of the various structures in the positive, neutral, and negative charge states. The electrical properties of the most stable configurations are calculated, and the charge-state dependent frequencies of the H- and C-related vibrational modes of the CH pair are predicted.

II. EXPERIMENT

A. Samples and measurement technique

The samples used here were FZ grown (100) oriented *n*- and *p*-type Si and relaxed $Si_{1-x}Ge_x$ crystals doped with P in the range of 5×10^{14}–4×10^{15} cm^{-3} or with B in the range of

2×10^{14}–2×10^{15} cm^{-3}, respectively. Ge concentrations were varied from $x = 0$ to 0.045 in the *n*-type samples and from $x = 0$ to 0.070 in the *p*-type material. The composition x was confirmed by energy-dispersive X-ray spectroscopy (EDX) measurements. The samples contained C_s at about 1×10^{15} cm^{-3}, as estimated from the C_s local-vibrational mode (LVM). Hydrogen was introduced by a remote dc-plasma at 313 K for 30 min (*n*-type), 373 K for 1 h (*p*-type), or by wet-chemical etching at room temperature for 10 min in an acid of HNO_3:HF:CH_3COOH with a 5:3:3 volume ratio. After hydrogenation, the samples were dipped in HF and Schottky diodes were produced by thermal evaporation in vacuum of Au (*n*-type) or Al (*p*-type) onto the polished side of the samples at room temperature. Ohmic contacts were prepared by rubbing the back side of the samples with a eutectic InGa alloy. The Schottky and Ohmic contacts were characterized by current-voltage (*IV*) and capacitance-voltage (*CV*) measurements in the range of 40–300 K. A Boonton 7200 capacitance bridge at 1 MHz was used for the *CV*-measurements.

Conventional DLTS spectra were recorded by using a lock-in amplifier with a rate window of 50 s^{-1}. Minority carrier injection (MCTS) measurements on etched samples with a thickness of ~100 μm were performed by back side illumination of the samples with the above band gap light of a laser diode. The Ohmic contacts at the back side covered only part of the surface and left enough space for light excitation. LDLTS with two filling pulses was employed to investigate the electronic properties of deep levels.[13] Laplace DLTS spectra were calculated from transients using the CONTIN method of the Tikhonov regularization, as described in Ref. 13. Trap concentrations and their depth profiles were calculated from the LDLTS spectra as described in Ref. 17. Isochronal annealing with short-circuited contacts was used to investigate the thermal stability of the defects. The levels are labeled using E or H (for electron or hole traps, respectively) followed by the temperature at which the peaks appear in the DLTS spectrum for an emission rate of 50 s^{-1}. If the fine structure in $Si_{1-x}Ge_x$ is considered, the labeling is followed either by (A) or (A$_n$), where A is the number of Ge atoms in the 1st and n in the 2nd NN shell of the defect, respectively.

B. Experimental results

1. The E90 level in n-type $Si_{1-x}Ge_x$ samples ($0 \leq x \leq 0.045$)

Wet-chemical etching at room temperature of *n*-type FZ-Si generates only the E90 level, as depicted in Fig. 2. Introducing H from a remote dc-plasma at or above 313 K generates the E262 and E42 DLTS levels with decreasing concentration of E90. Only E42 and E262 remain after a plasma treatment at 373 K. In CZ-Si, additional COH-related levels appear after hydrogenation.[18,19]

To investigate a possible correlation of the DLTS levels observed in *n*-type Si with those detected in *p*-type Si, DLTS and MCTS spectra were recorded from the same *n*-type FZ Si sample. Figure 3(a) presents the results obtained from a sample which was hydrogenated by wet-chemical etching. A single peak E90 is observed in the DLTS spectrum, while H180 appears in the MCTS spectrum. Due to a strong recombination outside the space charge region, hole injection is inefficient and only weak H180 signals could be detected. Figure 3(b) gives the DLTS and MCTS spectra of
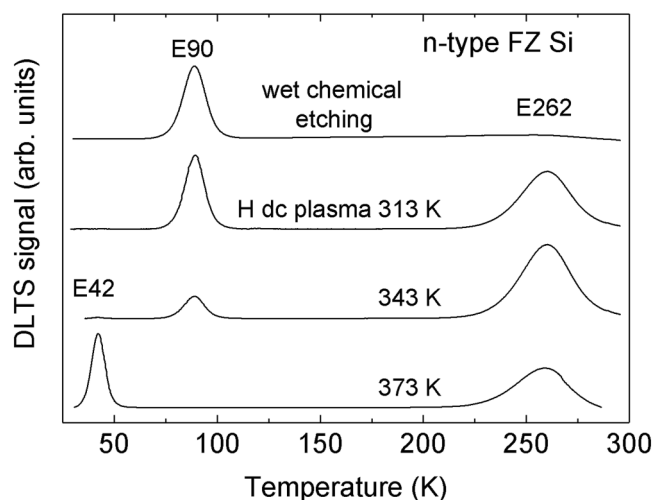
FIG. 2. DLTS spectra of *n*-type FZ Si after hydrogenation by wet-chemical etching or by a hydrogen dc-plasma at the indicated temperatures. The spectra were measured with $V_R = -1$ V, $V_P = 0$ V, a filling pulse width of 1 ms, and a rate window of 50 s^{-1}. Each spectrum is normalized to its maximum value and shifted vertically for clarity.

a sample cut from the same wafer as in Fig. 3(a) after hydrogenation by a H dc-plasma. In this sample, the dominant levels are E42 and E262 and the concentration of E90 is significantly lower. No MCTS peaks are observed in this sample [Fig. 3(b), bottom].

Several *n*-type Si$_{1-x}$Ge$_x$ samples with different compositions x were hydrogenated by a hydrogen dc-plasma at 313 K. The DLTS spectra are shown in Fig. 4(a). As discussed above, only the DLTS peak E90 is observed in pure Si ($x = 0$) at 90 K. In Si$_{0.989}$Ge$_{0.011}$, two peaks E90(0) at about 95 K and E90(1) at about 80 K are observed. The peak labeling anticipates our finding that E90(0) corresponds to the level E90 as observed in pure Si, while E90(1) is a CH pair like E90 but with one additional Ge atom in the 1st NN shell to C$_s$. When the Ge content in the samples is increased, both peaks shift to higher temperatures. In addition, the relative intensity of E90(1) with respect to E90(0) increases with increasing Ge concentration.

Figure 4(b) shows LDLTS spectra of the same samples recorded at 85 K. A single LDLTS peak E90 appears with an emission rate of 15 s^{-1} in Si ($x = 0$). In samples with $x > 0$, more complicated spectra are observed. Two dominant peaks labeled E90(0$_0$) and E90(1$_0$) are present in all spectra. They shift toward lower emission rates when the Ge concentration in the samples is increased. Besides these dominant peaks, several small satellites can be resolved. These satellites also shift with increasing x toward lower emission rates. The amplitudes and splittings relate them to the two dominant lines, and we label them 0$_1$ and 1$_1$, 1$_2$, and 1$_3$, respectively. The group of lines 0$_n$ ($n = 0$, 1) gives rise to the DLTS peak E90(0), whereas the lines 1$_n$ ($n = 0$ to 3) are responsible for the DLTS peak E90(1). With increasing Ge content, the relative concentration of all lines belonging to E90(1) increases with respect to that of E90(0).

The Arrhenius plots of the dominant LDLTS lines E90(0$_0$) and E90(1$_0$) recorded in samples with different concentrations of Ge are shown in Figs. 5(a) and 5(b). The values for the activation enthalpies E$_{na}$ and apparent capture cross sections σ_{na} are summarized in Table I. The activation enthalpies of both defect levels are found to be similar, but the apparent capture cross section of E90(1$_0$) is about one order of magnitude larger than that of E90(0$_0$). By increasing the Ge content, both the activation enthalpy and the apparent capture cross section of these defects remain approximately constant.

Figure 6 gives the depth profiles of E90 in pure Si (a) and E90(1$_0$) in a Si$_{0.974}$Ge$_{0.026}$ sample (b) after hydrogenation by wet-chemical etching. The profiles are compared to the depth dependence of the respective phosphorous–hydrogen (PH) pair in the two samples. The concentration of PH was calculated by subtracting the free carrier concentration after hydrogenation from the net free carrier concentration in the as-grown samples. In both samples, the PH and E90 profiles exhibit an identical decrease toward the bulk. Feklisova *et al.*[20] have demonstrated that, after hydrogenation by wet-chemical etching, the slope of the concentration profile of H-related defects is proportional to the number of H atoms in these complexes. The identical reduction of the concentration of E90/E90(1$_0$) and PH with depth clearly shows that, like the PH pair, E90/E90(1$_0$) contains a single hydrogen atom.

Figure 7 gives the change of the emission rates with electric field strength for E90 in Si and E90(0$_0$)/E90(1$_0$) for the Si$_{0.989}$Ge$_{0.011}$
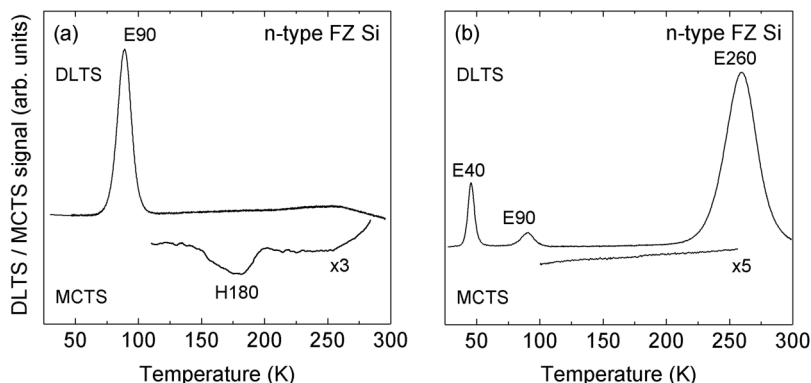
FIG. 3. Comparison of DLTS spectra (top) and MCTS spectra (bottom) recorded in *n*-type FZ Si after hydrogenation by (a) wet-chemical etching or (b) H dc-plasma treatment. The DLTS spectra were measured with $V_R = -2$ V, $V_P = 0$ V, a filling pulse width of 1 ms, and a rate window 50 s^{-1}. The MCTS spectra were measured with $V_R = -2$ V, a filling pulse width of 3 ms, and a rate window of 50 s^{-1}.
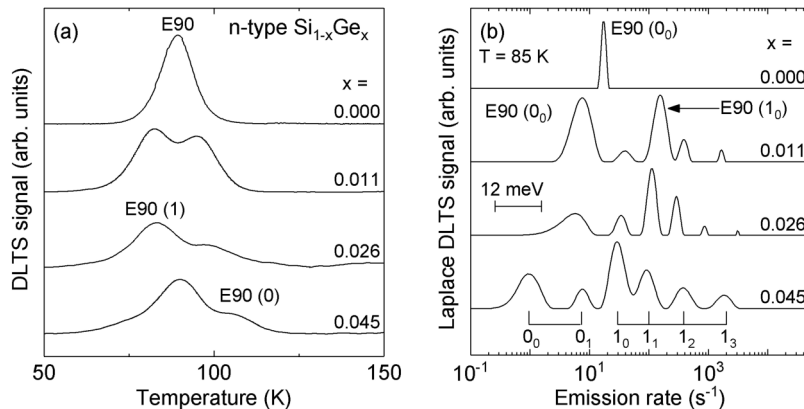
FIG. 4. DLTS (a) and LDLTS (b) spectra in *n*-type $Si_{1-x}Ge_x$ samples with different Ge concentrations *x* after hydrogenation by a hydrogen dc-plasma at 313 K. The 12 meV-energy scale corresponds to the enthalpy difference between $E90(0_0)$ and $E90(0_1)$, as calculated from the difference of the emission rates of these peaks under the assumption of a similar capture cross section.

sample. The levels show a weak dependence on the E-field strength. The full lines give the E^2-dependence of the emission rates, which is commonly explained by phonon-assisted tunneling.[21] The identical E-field dependence of both E90 lines supports their identification as the acceptor states of CH_{1BC} in environments with different Ge neighbors.

The thermal stability of E90 was investigated in hydrogen plasma treated samples by 15 min isochronal annealing steps performed with short-circuited contacts. After each annealing step, the concentration of the E90 defects was determined at the same depth. The results are shown in Fig. 8 for Si and $Si_{0.989}Ge_{0.011}$. The concentrations are normalized to their initial concentration N_0 measured at 85 K directly after hydrogenation. The concentration of E90 in Si is reduced by a factor of two at 340 K and anneals out at 360 K. $E90(0_0)$ and $E90(1_0)$ show a similar annealing behavior with a slightly higher stability of $E90(1_0)$ which anneals out at 380 K.

Figure 9 shows LDLTS spectra of the same sample with $x = 0.011$ recorded directly after hydrogenation (top) and after the annealing step at 370 K (bottom). Only the lines 1_n ($n = 0$ to 3) are seen after the annealing at 370 K with identical relative intensities compared to the as-prepared sample.

2. Level H180 in p-type $Si_{1-x}Ge_x$ samples $(0 \leq x \leq 0.07)$

Figure 10 presents DLTS spectra of a *p*-type CZ Si sample after hydrogenation by wet-chemical etching and by hydrogen dc-plasma at the indicated temperatures, respectively.

After wet-chemical etching, a single peak H50 and a weak H180 were detected. Besides H50, a minority carrier peak E262 shows up after hydrogen plasma treatment at 343 K. The dominant majority carrier peak H180 was observed only after a hydrogen plasma treatment at 373 K.

DLTS spectra recorded in *p*-type $Si_{1-x}Ge_x$ samples with $0 \leq x < 0.07$ after hydrogenation by a dc-plasma at 373 K are shown in Fig. 11(a). H180 is observed at about 180 K in pure Si. This peak shifts to lower temperatures and becomes asymmetrical with increasing Ge content. No other DLTS peaks appear in the $Si_{1-x}Ge_x$ samples in the investigated temperature range.

The LDLTS spectra of H180 recorded in the same samples at 170 K are presented in Fig. 11(b). In pure Si, a single LDLTS peak H180 is observed with an emission rate of $12 \, s^{-1}$. When the Ge content is increased, this peak [now labeled $H180(0)$ in the $Si_{1-x}Ge_x$ samples] broadens and shifts toward higher emission rates. In addition, a small satellite, labeled $H180(1)$, appears on the low frequency side of $H180(0)$ in the samples with $x \geq 0.046$.
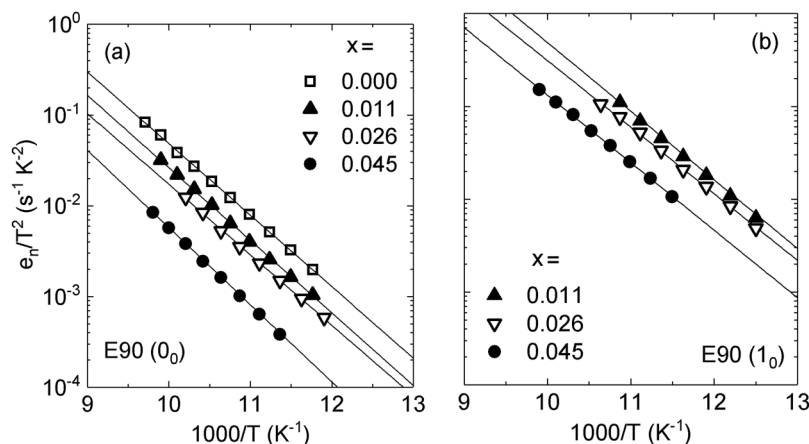
FIG. 5. Arrhenius plots of $E90(0_0)$ (a) and $E90(1_0)$ (b) in samples with different Ge concentrations.

TABLE I. Activation enthalpies and apparent capture cross sections of E90(0_0) and E90(0_1) measured in n-type Si$_{1-x}$Ge$_x$ samples with different Ge content.

Ge content x	E90(0_0)		E90(1_0)	
	E_{na} (meV)	σ_{na} (cm^2)	E_{na} (meV)	σ_{na} (cm^2)
0.000	160 ± 3	5.4×10^{-16}	…	…
0.011	158 ± 3	4.6×10^{-16}	152 ± 4	3.2×10^{-15}
0.026	155 ± 5	1.5×10^{-16}	145 ± 3	1.0×10^{-15}
0.045	167 ± 10	2.6×10^{-16}	144 ± 6	3.5×10^{-16}

With increasing Ge content, the intensity of this satellite increases with respect to H180(0).

Arrhenius plots of the LDLTS peak H180(0) in samples with different Ge content are given in Fig. 12. The activation enthalpies and apparent capture cross sections are summarized in Table II. In samples with higher Ge content, the activation enthalpy of the defect decreases, but the apparent capture cross section remains approximately constant in all samples. Due to the low concentration of H180(1), it was not possible to obtain a reliable Arrhenius plot for this level.

The capture cross section of H180 was directly measured in the temperature range of 170–210 K. A fit to a temperature dependent capture cross section $\sigma(T) = \sigma_\infty \exp\{-\Delta E_\sigma / k_B T\}$ gives a capture barrier of $\Delta E_\sigma = 53$ meV and $\sigma_\infty = 1.3 \times 10^{-16}$ cm^2. In combination with the results from the Arrhenius plot, this gives an activation energy for hole emission from H180 of $H_A = +(0.28 \pm 0.02)$eV. The emission rate of H180 in Si is independent of the electrical field strength below 2.2×10^4 V/cm.

Figure 13 shows the depth profiles of H180 and boron–hydrogen (BH) pairs recorded after wet-chemical etching of a p-type Si sample. The BH concentration was obtained by subtracting the free carrier concentration after hydrogenation from the net free carrier concentration in as-grown samples. The concentration of H180 and BH decrease toward the bulk with the same slope (logarithmic axis). According to Ref. 20, this is evidence that H180 contains a single H atom. Due to the broad linewidth of the LDLTS line H180(0) and the weakness of H180(0) in Si$_{1-x}$Ge$_x$, no depth profiles could be obtained from samples with $x > 0$.

Figure 14 gives the concentration changes of H180 after isochronal annealing. The sample was hydrogenated by a H dc-plasma at 100 °C, and after each 60-min annealing step, the concentration of H180 was determined always at the same depth.

III. THEORY

A. Methodology

Our spin-density-functional calculations use the SIESTA method[22,23] in Si$_{216}$ periodic supercells. The defect geometries are obtained with a conjugate gradient algorithm. A $3 \times 3 \times 3$ Monkhorst-Pack[24] mesh is used to sample the Brillouin zone. The electronic core regions are replaced by the Troullier–Martins norm-conserving pseudopotentials[25] developed for SIESTA.[26] The exchange-correlation potential is the revised generalized gradient approximation.[27] The charge density is projected on a real-space grid with an equivalent cutoff of 350 Ry to calculate the exchange-correlation and Hartree potentials. The basis sets for the valence states are linear combinations of numerical atomic orbitals:[28,29] double-zeta for H and C, with an additional set of d orbitals for Si.

The gap levels are evaluated using the marker method[30,31] with the perfect crystal as the universal marker for all the defects: the reference donor and acceptor levels are the top of the valence band and the bottom of the conduction band, respectively. This works well for a wide range of defects provided that the defect geometries and the lattice constant of the supercell are optimized in each charge state with a $3 \times 3 \times 3$ k-point sampling. This produces converged energies for the supercell size used here.

The activation energy for the reorientation of the CH pair was calculated using the nudged elastic band (NEB) method[32,33] in the Si$_{64}$ supercell with a $2 \times 2 \times 2$ Monkhorst–Pack mesh because of the substantial amount of computer time required in the NEB calculations. We use the climbing image method[34] for finding the saddle points. Local tangents are estimated using the improved-tangent formalism.[35] The springs connecting the images have a spring constant of 0.1 eV/Å. The converged path is the one for which the maximum force component perpendicular to the path at each image is less than 0.04 eV/Å.
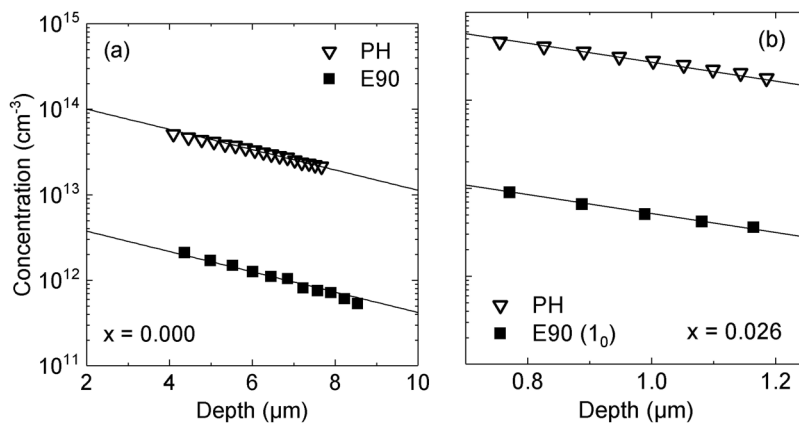
FIG. 6. Depth profiles of E90 (a) and E90(1_0) (b) together with the PH pair in the samples.
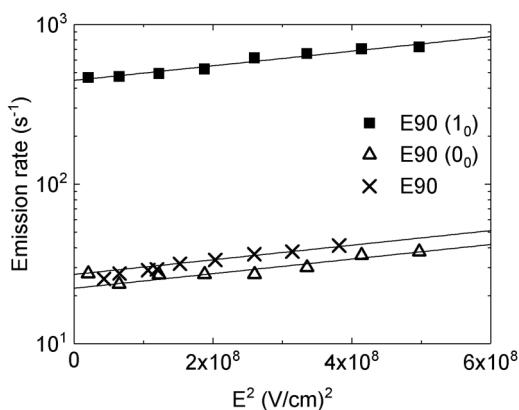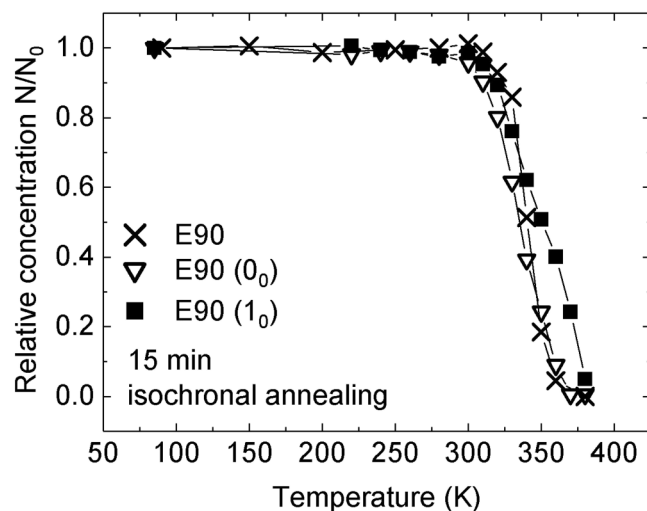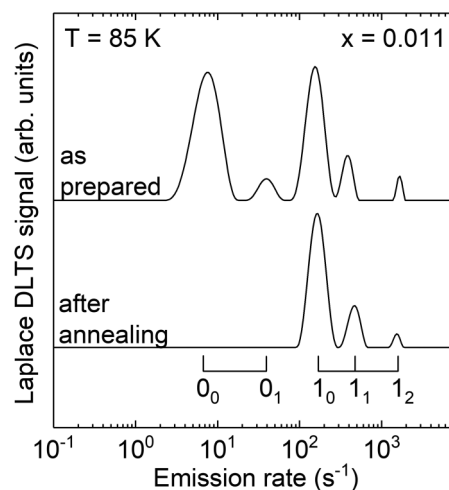
FIG. 7. The emission rate of E90 for $x = 0$ and E90(1_0), E90(0_0) for $x = 0.011$ as a function of the square of the electric field measured at 88 K. The lines are fits to the E^2-dependence of the phonon-assisted tunneling emission of carriers.[21]

FIG. 9. LDLTS spectra in the *n*-type $Si_{0.989}Ge_{0.011}$ sample after hydrogenation by a hydrogen dc-plasma at 313 K (top) and additional annealing at 370 K for 15 min (bottom) (compared to Fig. 8).

B. Theoretical predictions

Isolated C_s in Si is a substantial local perturbation because the equilibrium C—Si bond length is substantially shorter than the Si—Si one. Thus, C_s attracts its four Si NNs and, in the optimized geometry, C_s—Si_{NN} = 2.041 Å (as compared to Si—Si = 2.384 Å in the perfect Si_{216} supercell). By itself, C_s is electrically inactive in Si and remains in the 0 charge state for all positions of the Fermi level. However, the strain associated with it attracts interstitial H, which binds directly to carbon. This relieves some of the strain

around it. Further, since the C—H bond is stronger than the Si—H one (e.g., it is about 4.3 eV in methane vs 4.1 in silane) H binds more strongly to C than to Si in C-H-Si.

Geometry optimizations have been performed for H at all the sites shown in Fig. 1 for the CH pair in the positive, neutral, and

FIG. 8. Normalized concentrations of E90(0_0) and E90(1_0) in $Si_{0.989}Ge_{0.011}$ after isochronal annealing for 15 min with short-circuited contacts. For comparison, the concentration of E90 in a Si sample (annealed under the same conditions) is given. The lines connecting the experimental points are guide to the eye.
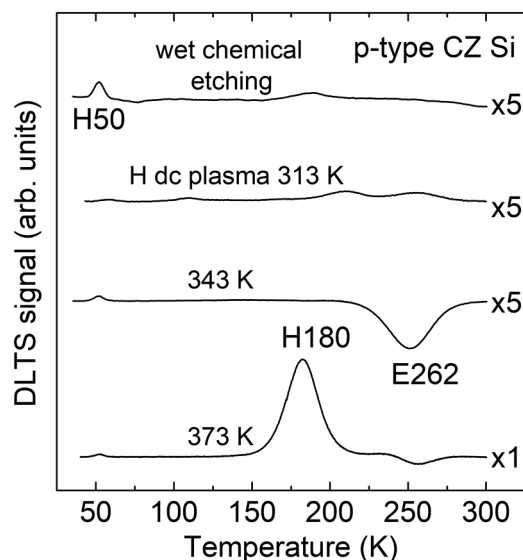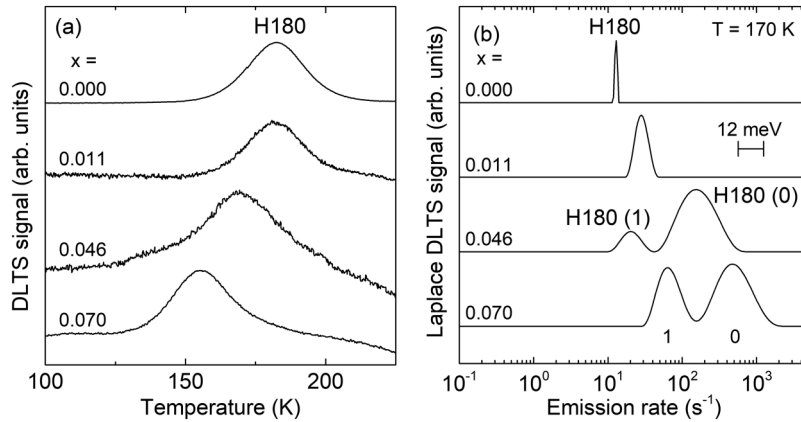

FIG. 10. DLTS spectra from a *p*-type CZ Si sample ([C_s] = 6 × 10^{17} cm^{-3}, [O_i] = 7 × 10^{17} cm^{-3}) after hydrogenation by wet-chemical etching or H dc-plasma treatment for 45 min at the indicated temperatures. The spectra were recorded with V_R = −2 V, V_P = 0 V, a filling pulse width of 1 ms, and a rate window of 50 s^{-1}.

FIG. 11. (a) DLTS spectra of p-type $Si_{1-x}Ge_x$ samples with different Ge content x after hydrogenation by a dc-plasma treatment at 373 K. (b) LDLTS spectra of the same samples. The energy scale of 12 meV serves to compare the energy resolution with that of Fig. 4(b).

negative charge states. The lowest-energy configurations are in good agreement with those found by Santos et al.[19] In the +1 charge state, the lowest-energy configuration is CH_{1BC}, albeit with a small binding energy relative to isolated bond-centered hydrogen: $Si_{215}C_s^0 + Si_{216}H_{BC}^+ \rightarrow Si_{215}CH_{1BC}^+ + Si_{216}^0$ with an energy gain of just 0.38 eV. In the 0 charge state, the lowest-energy configuration is also CH_{1BC}, with a binding energy (relative to isolated H_{BC}^0) of 0.90 eV. Finally, in the −1 charge state, two configurations are nearly degenerate. We find CH_{1AB} to be 0.04 eV lower than CH_{1BC}, and $Si_{215}C_s^0 + Si_{216}H_T^- \rightarrow Si_{215}CH_{1AB}^- + Si_{216}^0$ with an energy gain of 0.54 eV. We will focus on these configurations because other a priori possible metastable configurations have near zero or even negative binding energies making them highly unlikely that they would

occur. Figure 15 shows the geometry-optimized CH_{1BC} and CH_{1AB} configurations.

We performed a NEB calculation to determine that reorientation barrier of H from CH_{1BC}^- to CH_{1AB}^- and obtained 1.4 eV, which is much larger than the binding energy. The reason for this large barrier is that C_s must move across the plane of its three Si NNs in order for H to bind to it at the AB site. It is, therefore, highly unlikely that H would ever successfully reorient from the BC to the AB configuration. If the CH pair pair forms in strongly n-type Si, some of the H would be CH_{1AB}^- and the rest CH_{1BC}^-, but if the pair forms in intrinsic or p-type Si, it would always be CH_{1BC}^0 or CH_{1BC}^+.

We calculated the gap levels of the CH pair assuming that it always stays in the CH_{1BC} configuration or always in the CH_{1AB} configuration, since the reorientation between the two is highly unlikely. For CH_{1BC}, we calculate the donor level to be at $E_V + 0.27$ eV (0.28) and the acceptor level at $EC−0.18$ eV (0.17) (the numbers in parenthesis are those obtained by Santos et al.[19] For CH_{1AB}, we find the donor level at E_v of + 0.11 eV and the acceptor level at $EC−0.62$ eV. The calculated acceptor level of CH_{1AB} is in fair agreement with the experimental value of $EC−0.51$ eV.[12]

Finally, we calculated the force-constant matrix in the lowest-energy configuration for each charge state and the dynamical matrices for the CH and CD modes (Fig. 16). These LVMs have not yet been measured or calculated. The eigenvalues of the dynamical matrix are the normal mode frequencies ω_s. The
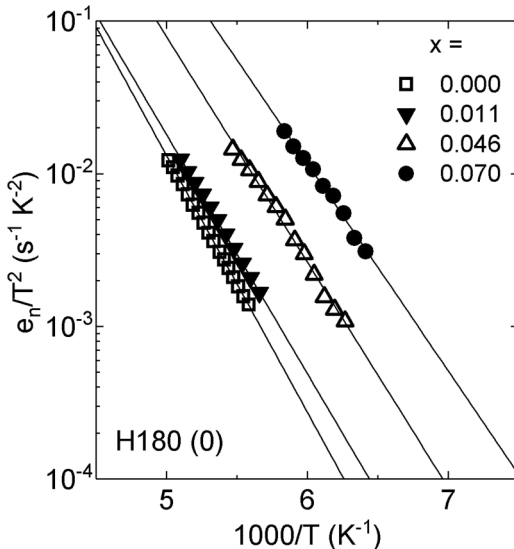
FIG. 12. Arrhenius plots of H180(0) obtained in p-type $Si_{1-x}Ge_x$ samples with varying Ge content x.

TABLE II. Activation enthalpies and apparent capture cross sections of H180(0) measured in p-type $Si_{1-x}Ge_x$ samples with different Ge content.

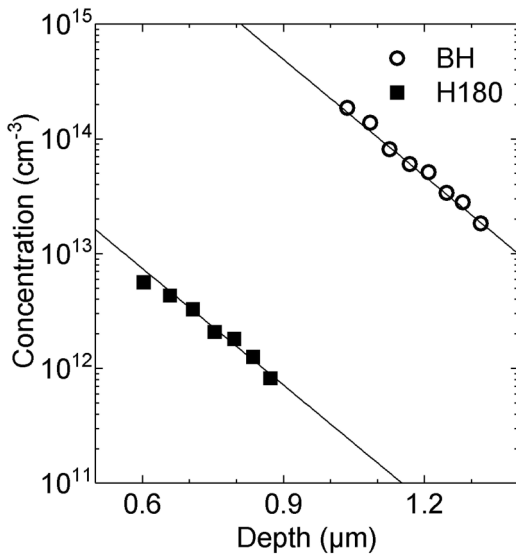|	H180(0)	
Ge content x	E_{na} (meV)	σ_{na} (cm^2)
0.000	333 ± 2	1.7×10^{-16}
0.011	310 ± 4	3.5×10^{-16}
0.046	293 ± 7	2.7×10^{-16}
0.070	270 ± 10	2.3×10^{-16}

FIG. 13. Depth profile of H180 and BH in a p-type Si sample after wet-chemical etching. ($[N_d] = 1 \times 10^{15}$ cm^{-3}, $[C_S] = 6 \times 10^{17}$ cm^{-3}, $[O_i] = 7 \times 10^{17}$ cm^{-3}).

corresponding orthonormal eigenvectors $e^s_{\alpha i}$ (where i = x,y,z) give the relative displacements of the nucleus α for each mode s. A quantitative measure of the localization of a given mode on one atom or group of atoms is given by a plot of $L^2_{\{\alpha\}} = (e^s_{\alpha x})^2 + (e^s_{\alpha y})^2 + (e^s_{\alpha z})^2$ vs ω, with $0 < L^2 < 1$. The index $\{\alpha\}$ may be a single atom (e.g., H) or a sum over a group of atoms (e.g., the Si nearest neighbors to H). Figure 15 show plots of L^2 for CH^+_{1BC} (top), CH^0_{1BC} (middle), and CH^-_{1AB} (bottom) for $\{\alpha\}$ = H, C, and the Si atom along the C–H axis. Table III lists the most important modes for CH^+_{1BC}, CH^0_{1BC}, CH^-_{1BC}, and CH^-_{1AB}, including D substitutions.
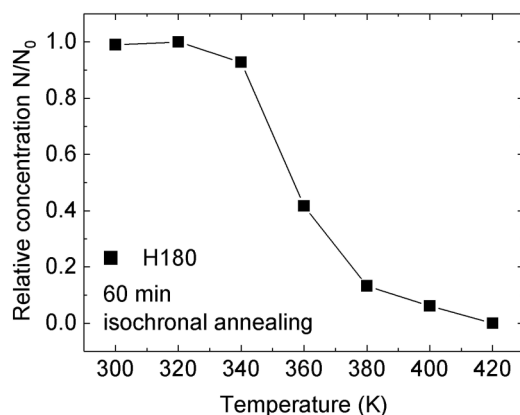

FIG. 14. Normalized concentration of H180 in a Si sample after isochronal annealing in 60-min steps with short-circuited contacts.
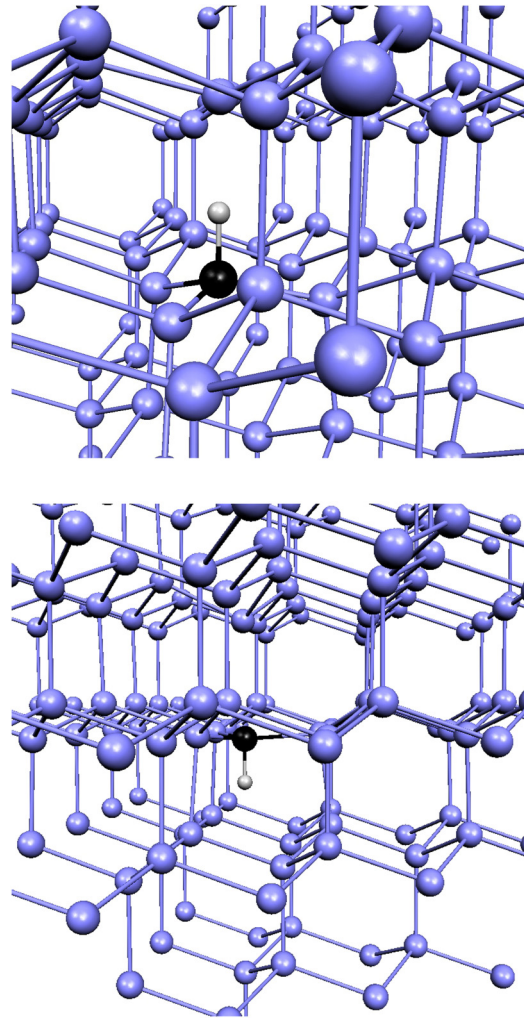

FIG. 15. The lowest-energy configuration of the CH pair in the +1 and 0 charge states is CH_{1BC} (top) and in the −1 charge state it is CH_{1AB} (bottom), albeit only by 0.04 eV relative to CH_{1BC}. The Si atoms are light blue (gray), C is the small black ball, and H is the white ball. The large reorientation barrier (see the text) between the two configurations shows that the CH_{1AB} configuration is likely to be realized only when the pair originally forms in heavily n-type Si.

IV. DISCUSSION

The DLTS peaks E90 and H180 were only seen in n- and p-type Si and SiGe alloys following hydrogenation. The E90 peak is commonly attributed to CH_{1BC} but has been assigned to a donor[2,4] as well as to an acceptor level.[6] This contradiction could be resolved by LDLTS measurements.[7] Two levels (E90 and E90′) separated by only ~20 meV were identified as the acceptor state of CH_{1BC} (E90) and a donor state (E90′) of a CH defect which contains at least two hydrogen atoms. The electrical properties of E90 (activation enthalpy and apparent capture cross section) are similar to those reported in Refs. 6 and 11, and the level position agrees well with our calculations.
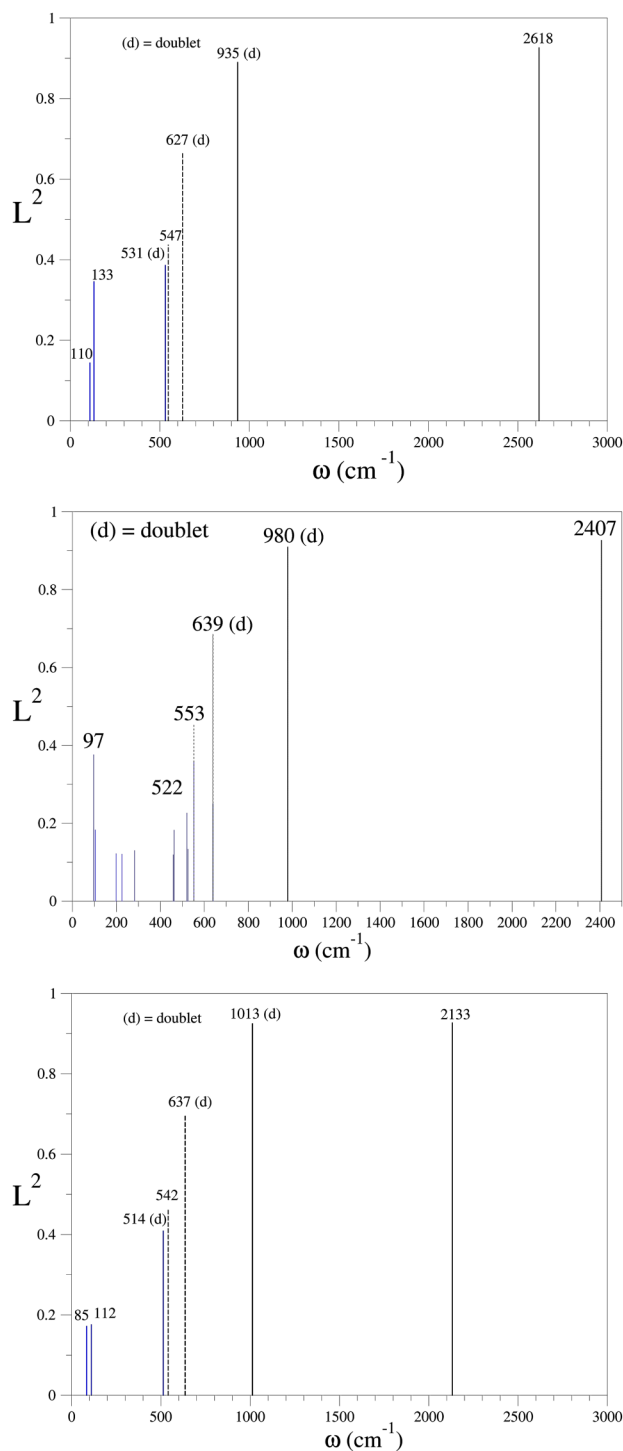
FIG. 16. Plots of the localization L^2 (vertical axis, see the text) showing the H- (solid black), C- (dotted black), and Si- (blue) related modes for the CH_{1BC}^+ (top), CH_{1BC}^0 (middle), and CH_{1AB}^- (bottom) pairs. The horizontal axis is the frequency ω in cm^{-1}.

TABLE III. Calculated H- (2nd column) and C-related (3rd column) LVM frequencies (cm^{-1}) for CH_{1BC}^+, CH_{1BC}^0, CH_{1BC}^-, and CH_{1AB}^-. The higher of the two frequencies are stretch modes and the lower are (doublet) wag modes. The numbers in parenthesis correspond to D substituting H. Only the frequencies above the optical phonon of Si ($\sim$530 cm^{-1}) are listed.

CH_{1BC}^+	2618 (1921)	627 (540)
	935 (721)	547
CH_{1BC}^0	2407 (1766)	639 (670)
	980 (744)	553 (544)
CH_{1BC}^-	2147 (1565)	656 (614)
	1012 (760)	550 (533)
CH_{1AB}^-	2133 (1565)	637 (614)
	1013 (760)	542 (533)

The depth profiles of E90 and the neutral PH pair recorded after wet-chemical etching at room temperature (Fig. 6) identify E90 as a CH pair with only one hydrogen atom.[20] E90 exhibits a weak enhancement of the emission rate with electric field, which is in agreement with the phonon-assisted tunneling from a neutral center (acceptor state in the upper half of the bandgap).[21] In agreement with the calculated level position, our measurements confirm the identification of E90 as being associated with the CH_{1BC} pair.

The thermal stability of this pair can be estimated from the isochronal annealing curve (Fig. 8). Under the assumption of a first-order reaction with an attempt frequency of typical lattice phonons in Si, we obtain a thermal barrier of $\sim$1.0 eV. E90 is not formed in samples treated in a hydrogen dc-plasma at temperatures above 373 K, consistent with the calculated binding energies for CH_{1BC}. We could not detect a direct conversion from E90 to E42/E262, which have previously been associated with the CH_{1AB} configuration.[12] The large thermal barrier seems to be associated with the thermal dissociation of the CH_{1BC} pair. According to our calculations, the direct transfer of E90 into the CH_{AB} configuration is associated with an even higher barrier.

The H180 peak has been assigned by Kamiura et al. to the donor state of the CH_{1AB} configuration or a CH pair with more than one hydrogen atom.[4] Our depth profiles of H180 and the BH pairs in the same sample (Fig. 13) identify H180 as being associated with a defect that contains only one hydrogen atom. The appearance of H180 in the MCTS spectrum of Fig. 3(a) strongly supports that E90 and H180 belong to the same CH_{1BC} center.

Based on the absence of an enhancement of the emission rate with electric field, Kamiura et al. identified H180 as a deep donor state.[4] Our study confirms the lack of an E-field dependence on the emission rate. The detected capture barrier indicates a strong electron–phonon coupling in the different charge states of the defect. The support for an acceptor state presented in Ref. 15—which is based on the idea that the capture barrier could hinder the emission rate enhancement of the electric field[36]—is not valid in the present case.

H180 is thermally destroyed around 100 °C, which is similar to the results of Kamiura et al.[4] An approximate thermal energy of $\sim$1.4 eV is derived from our isochronal annealing measurements

(first-order process with an attempt frequency of $\sim 10^{13}\,\mathrm{s}^{-1}$), somewhat smaller than the 1.7 eV determined directly from isothermal annealing.[4] We associate H180 with the donor state of the CH_{1BC} defect based on the calculated energy-level position, the involvement of a single H, and the field independence of the emission rate.

In diluted n-type and p-type $Si_{1-x}Ge_x$ alloys, the DLTS peaks E90 and H180 split, show shoulders, and shift with x. With the higher resolution of LDLTS, we observe clearly resolved peaks [Figs. 4(b) and 11(b)]. The depth profiles in Fig. 6 show that E90 (1_0) and E90(0_0) contain a single hydrogen atom. Both levels have similar thermal stabilities (Fig. 8) and activation enthalpies (Table I). Furthermore, the LDLTS peak E90(1_0) and the satellites [Fig. 4(b)] only appear in $Si_{1-x}Ge_x$ samples, and with respect to E90(0_0) their intensities increase with the Ge content. Previously, the presence of Ge in the 1st and 2nd NN shells around Fe, FeB, Au, and Pt in $Si_{1-x}Ge_x$ alloys resulted in the appearance of similar additional LDLTS peaks.[14,37] In agreement with these studies, we correlate the peaks with defects, which have different numbers of Ge atoms in their vicinity.

We assign E90(0_0) to CH_{1BC} with no Ge atoms in its 1st or 2nd NN shells, whereas E90 (1_0) is attributed to CH_{1BC} with one Ge atom in the 1st shell and no Ge atom in the 2nd shell. By analogy, we assign the configurations that have more Ge atoms in the 2nd shell E90(0_n) and E90(1_n) with $n = 1$, 2, or 3. In contrast to the results presented in Fig. 4(b), for H180, it is not possible to resolve defects with a different number of Ge atoms in the 2nd NN shell. This can be explained by the lower resolution of LDLTS at this temperature, compared to the measurements at 85 K. To illustrate this, the splitting between E90(0_0) and E90(0_1) of about 12 meV [see Fig. 4(b)] is included in Fig. 11(b).

The emission rates of H180(0) and H180(1) were found to differ by a factor of about eight. Under the assumption of similar apparent capture cross sections, this translates into $k_BT\ln(e_1/e_0) \sim 20$ meV. This value is similar to the energy difference between E90(0_0) and E90(1_0), which differ only by the number of Ge atoms in their 1st shell. In addition, the observed energy separation (~ 12 meV) between peaks that differ by one Ge atom in the 2nd shell [E90(1_n)] corresponds approximately to the full width at half maximum (FWHM) of the LDLTS peak H180(0). These arguments lead us to assign H180(0) and H180(1) to CH pairs with no or one Ge atom in the 1st shell, respectively. The components with additional Ge atoms in the 2nd shell are hidden under the broad LDLTS peaks and cannot be resolved at 180 K.

In order to analyze quantitatively the intensities of the dominant peaks and their satellites [Figs. 4(b) and 11(b)], we have to calculate the probability of finding 0, 1, 2, or 3 Ge atoms in the 1st and 2nd NN shells of CH_{1BC}. We assume a random distribution of Ge in our relaxed $Si_{1-x}Ge_x$ alloys, as previously confirmed by XAFS measurements[38] and mutually independent distributions of Ge and C. The latter was confirmed by Hoffmann *et al.*, who detected a purely statistical distribution of Si and Ge atoms around C_s in diluted $Si_{1-x}Ge_x$ samples with x < 0.05.[39]

C_s in Si is known to introduce a strong bond-length mismatch. Binding additional Ge to the Si—C structure increases that mismatch.[39] A similar increase is detected for the Ge—C bond, if additional Si atoms bind to the structure. Hoffmann *et al.* detected a substantial preference for the formation of C complexes with many (3 or 4) Si neighbors in their $Si_{1-x}Ge_x$ samples. However, for values x < 0.05, the authors detect a purely statistical distribution of Si and Ge atoms around C_s. In contrast, hydrogen is expected to be preferentially captured in the highly strained C—Si or C—Ge bonds, which allows C_s to shorten three of its four bonds at a substantial gain in energy.[9]

Under these conditions, the probability of finding Ge as one of the NN sites can be calculated from the binomial distribution. The calculations require a model of the local environment of the defect which defines the number of sites adjacent to CH. In the present context, a certain neighborhood (1st NN, 2nd NN…to C_s) is defined as the set of all atoms that are energetically equivalent with respect to substitution. The term *energetically equivalent* means that occurring differences in energy are smaller than the resolution limit of the measurement technique.

Since we do not know if H binds preferably to a C—Si or C—Ge bond, we test two different models of the local environment of the CH defect. The "4NN" model, sketched in Fig. 17(a), assumes that the 1st NN shell of CH_{1BC} is determined by the four 1st-NNs of C_s (1st shell). The 2nd NN shell contains 12 atoms. The "6NN" model, illustrated in Fig. 17(b), is tailored for a defect configuration with a preferential binding of H to a C—Si bond. In this case, the 1st shell contains 6 atoms and the 2nd shell contains a total of 18 atomic sites.

The calculated distributions for the two models are compared in Fig. 18 to the defect concentrations determined from the LDLTS measurements on E90, given in Fig. 4(b). The experimental concentrations of E90(A_n) (gray bars) and the calculated probabilities for the occupation of the neighboring lattice sites of C with Ge (dashed bars) in the "4NN" model are compared in Fig. 18 (top) and to the "6NN" model in Fig. 18 (bottom). The calculated probabilities are normalized to the concentration of the (0_0) defect configuration.
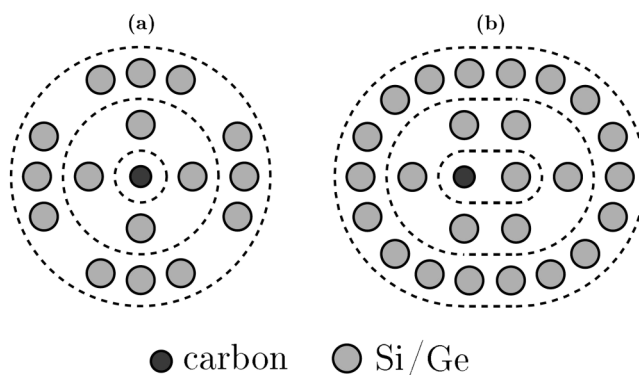
FIG. 17. The 1st and 2nd NN shells of C_s in the frame of the "4NN" model (left) with 4 and 12 atoms around CH_{1BC}, and the "6NN" model (right) with 6 and 18 atoms around CH_{1BC}.
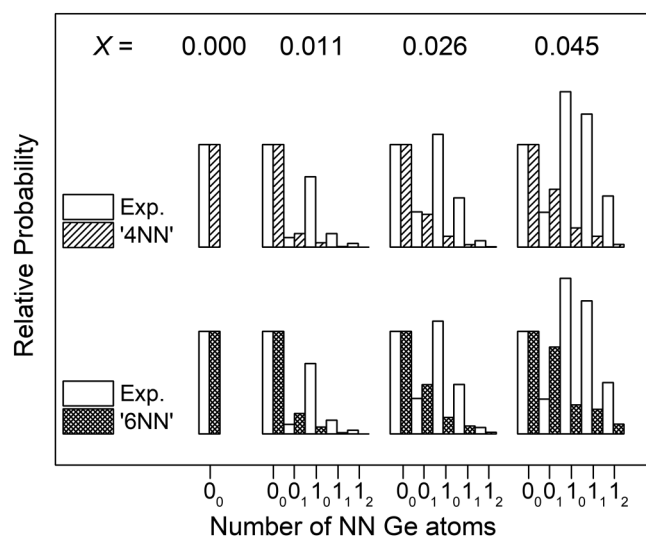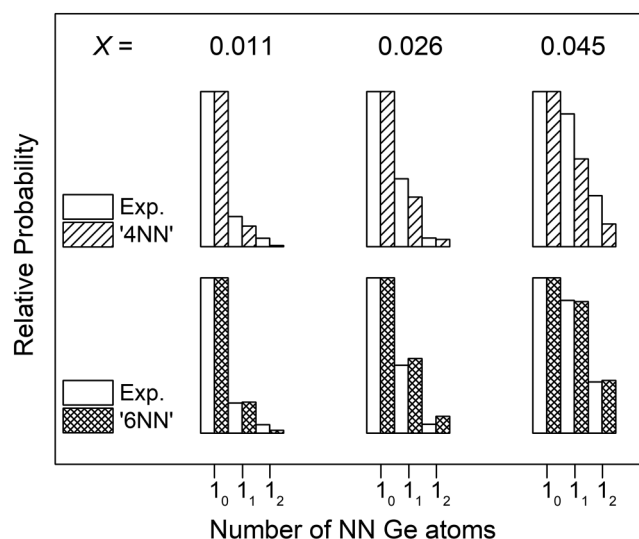
FIG. 18. Comparison of the experimental concentrations of E90(A_n) and the calculated probabilities of finding Ge atoms in the 1st and 2nd NN shells of the CH_{1BC} pair assuming the "4NN" (top) and the "6NN" (bottom) models. The probabilities are normalized to the experimental concentration of 0_o.

FIG. 19. Comparison of the experimental concentrations of E90(1_n) and the calculated probabilities of finding Ge atoms in the 2nd NN shell CH_{1BC} in the "4NN" (top) and "6NN" (bottom) models. Probabilities are normalized to the experimental concentration of E90(1_0).

The simulation of the Ge distribution for the "4NN" as well as the "6NN" models deviate from the experimental defect concentrations. Obviously, there is a strong preference of H to bind to those complexes which have a Ge atom in the 1st shell (1_n).

In Fig. 19, we compare the experimental concentrations of only E90(1_n) (gray bars) with the calculated Ge distribution in the 2nd NN shell around C_s in the "4NN" model (top) and the "6NN" model (bottom). The concentrations are now normalized to E90 (1_0). Here, excellent agreement between the experimental data and the calculated Ge distribution is observed in the case of the "6NN" model, whereas the predictions of the "4NN" model are always smaller than the experimental values. This result shows that the distribution of Ge in the second-nearest shell of E90(1_n) can be accurately described if one assumes a bond-centered structure of this defect. This finding is consistent with the assumed origin of E90(1_n) as the CH_{1BC} configuration with one Ge atom in its first-NN shell.

In Fig. 20, we compare the experimentally detected concentrations of H180(0) and H180(1) observed in p-type $Si_{1-x}Ge_x$ to the calculated probabilities of the "4NN" and "6NN" models. The calculated probabilities are normalized to the experimental concentration of H180(0). The absence of a large preferential formation of defects with one Ge atom in their 1st shell is in strong contrast to the results obtained for E90 in n-type $Si_{1-x}Ge_x$.

The observed difference between the n-type and p-type samples cannot be explained by their different doping concentrations. E90(A_n) and H180(A) were observed in samples after hydrogenation at 295–373 K. In this temperature range, the position of the Fermi level varies from 0.26 eV to 0.34 eV from the conduction band [i.e., below the E90(A_n) level] in n-type samples, and it is in the range of 0.25 eV–0.33 eV from the valence band [i.e., above the

H180(A) level] in p-type $Si_{1-x}Ge_x$. At these positions of the Fermi level, CH_{1BC} should be in the 0 charge state, and a significant part of interstitial H should be always positively charged.[40] Therefore, the formation of hydrogen complexes should be identical in our
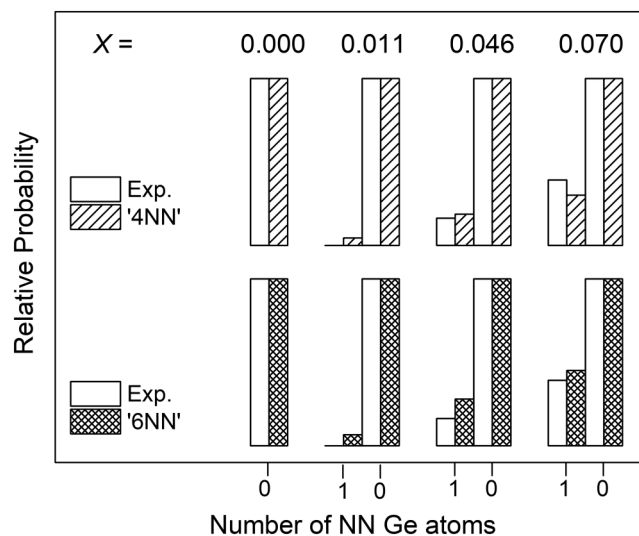
FIG. 20. Comparison of the experimental concentrations of H180(A) with the calculated probabilities of finding Ge atoms in the 1st NN shell of CH_{1BC} evaluated in the "4NN" (top) and "6NN" (bottom) models, respectively. Probabilities are normalized to the experimental concentration of H180(0).

samples. If E90(A_n) and H180(A) belong to the same defect, one would intuitively expect identical patterns of the LDLTS lines.

Strong support that E90 and H180 belong to the same CH_{1BC} defect comes from the presented calculations and the MCTS spectra. If we accept that E90 and H180 belong to the same CH_{1BC} structure, an explanation is needed for the preferential binding of E90 to Ge atoms in the 1st NN shell. In a simplistic model of the defect structure, the CH_{1BC}^+ structure consists of a H atom strongly bound to C_s with two electrons in the C—H bonding orbital and an empty dangling bond associated with the nearby Si atom along the trigonal axis. In the neutral charge state, this dangling bond contains one electron. In the negative charge, two electrons occupy this orbital which repels H and leads to a strongly-strained defect structure. A Ge atom in the 1st NN shell contributes to a larger relaxation of the C atom and, therefore, to a preferential binding of the negatively charged CH_{1BC} defect. This model of a strain relaxation of the negatively charged pair by nearby Ge atoms would support a preferential binding of H in the CH_{1BC} configuration with Ge in the 1st shell. The neutral and positively charged complexes do not experience such a strong strain relaxation and, therefore, display a purely statistical distribution of the defect configurations.

V. CONCLUSIONS

Our DLTS and MCTS study on E90 and H180 and in n- and p-type Si after hydrogenation relate these levels to acceptor and donor states of a CH defect. The presence of Ge atoms in $Si_{1-x}Ge_x$ alloys modifies the electrical properties of the CH pair (E90 and H180) and results in the appearance of additional defects with different numbers of Ge atoms in their 1st and 2nd NN shells. Calculations show that E90 and H180 are the donor and acceptor levels of CH_{1BC}. The LVM theoretically predicted here should help further confirmation from FTIR experiments. The pattern of the LDLTS spectra of E90 and H180 in $Si_{1-x}Ge_x$ alloys and their annealing behavior support that these levels belong to the same CH_{1BC} defect, if we include for the negatively charged complex a preferential binding of hydrogen to CH_{1BC} pairs with at least one Ge in the 1st NN shell.

ACKNOWLEDGMENTS

REFERENCES

[1]B. O. Kolbesen and A. Mühlbauer, Solid State Electron. **25**, 759 (1982).
[2]A. Endrös, Phys. Rev. Lett. **63**, 70 (1989).
[3]W. Csaszar and A. L. Endrös, Phys. Rev. Lett. **73**, 312 (1994).
[4]Y. Kamiura, M. Tsutsue, Y. Tamashita, F. Hashimoto, and K. Okuno, J. Appl. Phys. **78**, 4478 (1995).
[5]L. Hoffmann, E. V. Lavrov, B. B. Bech Nielsen, B. Hourahine, R. Jones, S. Öberg, and P. R. Briddon, Phys. Rev. B **61**, 16659 (2000).

[6]O. Andersen, A. R. Peaker, L. Dobaczewski, K. B. Nielsen, B. Hourahine, R. Jones, P. R. Briddon, and S. Öberg, Phys. Rev. B **66**, 235205 (2002).
[7]R. Stübner, V. Kolkovsky, and J. Weber, J. Appl. Phys. **118**, 055704 (2015).
[8]P. Leary, R. Jones, and S. Öberg, Phys. Rev. B **57**, 3887 (1998).
[9]D. M. Maric, P. F. Meier, and S. K. Estreicher, Phys. Rev. B **47**, 3620 (1993).
[10]C. Kaneta and H. Katayama-Yoshida, Mater. Sci. Forum **196–201**, 897 (1995).
[11]M. Yoneta, Y. Kamiura, and F. Hashimoto, J. Appl. Phys. **70**, 1295 (1991).
[12]R. Stübner, L. Scheffler, V. Kolkovsky, and J. Weber, J. Appl. Phys. **119**, 205709 (2016).
[13]L. Dobaczewski, A. R. Peaker, and K. B. Nielsen, J. Appl. Phys. **96**, 4689 (2004).
[14]L. Dobaczewski, K. Goscinski, K. Bonde Nielsen, A. Nylandsted Larsen, and J. Lundsgaard Hansen, Phys. Rev. Lett. **83**, 4582 (1999).
[15]R. Stübner, V. Kolkovsky, L. Scheffler, and J. Weber, Phys. Status Solidi C **13**, 770 (2016).
[16]R. Stübner, V. Kolkovsky, J. Weber, and N. V. Abrosimov, Phys. Status Solidi A **214**, 1700329 (2017).
[17]P. Blood and P. W. Orton, *The Electrical Characterization of Semiconductors Majority Carriers and Electron States* (Academic Press, London, 1992).
[18]K. Gwozdz, R. Stübner, V. Kolkovsky, and J. Weber, Appl. Phys. Lett. **111**, 032102 (2017).
[19]P. Santos, J. Coutinho, S. Öberg, M. Vaqueiro-Contreras, V. P. Markevich, M. P. Halsall, and A. R. Peaker, Phys. Status Solidi A **214**, 1700309 (2017).
[20]O. V. Feklisova, E. B. Yakimov, and N. A. Yarykin, Semiconductors **36**, 282 (2002).
[21]S. D. Ganichev, E. Ziemann, W. Prettl, I. N. Yassievich, A. A. Istratov, and E. R. Weber, Phys. Rev. B **61**, 10361 (2000).
[22]D. Sánchez-Portal, P. Ordejón, E. Artacho, and J. M. Soler, Int. J. Quant. Chem. **65**, 453 (1997).
[23]E. Artacho, D. Sánchez-Portal, P. Ordejón, A. García, and J. M. Soler, Phys. Status Solidi B **215**, 809 (1999).
[24]H. J. Monkhorst and J. D. Pack, Phys. Rev. B **13**, 5188 (1976).
[25]N. Troullier and J. L. Martins, Phys. Rev. B **43**, 1993 (1991).
[26]P. Rivero, V. M. García-Suárez, D. Pereñiguez, K. Utt, Y. Yang, L. Bellaiche, K. Park, J. Ferrer, and S. Barraza-Lopez, Comput. Mater. Sci. **98**, 372 (2015).
[27]B. Hammer, L. B. Hansen, and J. K. Nørskov, Phys. Rev. B **59**, 7413 (1999).
[28]O. F. Sankey and D. J. Niklevski, Phys. Rev. B **40**, 3979 (1989).
[29]O. F. Sankey, D. J. Niklevski, D. A. Drabold, and J. D. Dow, Phys. Rev. B **41**, 12750 (1990).
[30]A. Resende, R. Jones, S. Öberg, and P. R. Briddon, Phys. Rev. Lett. **82**, 2111 (1999).
[31]J. P. Goss, M. J. Shaw, and P. R. Briddon, in *Theory of Defects in Semiconductors*, edited by D. A. Drabold and S. K. Estreicher (Springer, Berlin, 2007), p. 69.
[32]G. Mills and H. Jonsson, Phys. Rev. Lett. **72**, 1124 (1994).
[33]H. Jonsson, G. Mills, and K. W. Jacobsen, in *Classical and Quantum Dynamics in Condensed Phase Simulations*, edited by B. J. Berne, G. Ciccotti, and D. F. Coker (World Scientific, Singapore, 1998), p. 385.
[34]G. Henkelman, B. P. Uberuaga, and H. Jonsson, J. Chem. Phys. **113**, 9901 (2000).
[35]G. Henkelman and H. Jonsson, J. Chem. Phys. **113**, 9978 (2000).
[36]W. R. Buchwald and N. M. Johnson, J. Appl. Phys. **64**, 958 (1988).
[37]V. Kolkovsky, A. Mesli, L. Dobaczewski, N. V. Abrosimov, Z. R. Żytkiewicz, and A. R. Peaker, Phys. Rev. B **74**, 195204 (2006).
[38]I. Yonenaga, J. Cryst. Growth **275**, 91 (2005).
[39]L. Hoffmann, B. Bech Nielsen, A. Nylandsted Larsen, P. Leary, R. Jones, P. R. Briddon, and S. Öberg, Phys. Rev. B **60**, 13573 (1999).
[40]C. Herring, N. M. Johnson, and C. G. Van de Walle, Phys. Rev. B **64**, 125209 (2001).